Int J Clin Exp Med 2015;8(3):3349-3359
www.ijcem.com /ISSN:1940-5901/IJCEM0005415

Original Article

Temporal and spatial changes in VEGF, αA- and αB-crystallin expression in a mouse model of oxygen-induced retinopathy

Yi Shi*, Chang Su*, Jian-Tao Wang, Bei Du, Li-Jie Dong, Ai-Hua Liu, Xiao-Rong Li

*Tianjin Medical University Eye Hospital, School of Optometry and Ophthalmology, Tianjin Medical University Eye Institute, Tianjin Medical University, Tianjin 300384, China. *Equal contributors.*

Received December 31, 2014; Accepted February 28, 2015; Epub March 15, 2015; Published March 30, 2015

Abstract: Objective: Retinal neovascularization is an iconic change in retinopathies. Vascular Endothelial Growth Factor (VEGF) and α-crystallins have been identified to mediate the pathogenesis of retinopathy. However, the special and temporal changes in their expression associated with retinal neovascularization have not yet been determined. Therefore, we examined the expression and distribution of VEGF, αA- and αB-crystallins in the retina using a mouse model of oxygen-induced retinopathy (OIR). Methods: 90 C57/BL mice were randomly divided into the OIR and control groups. The OIR group at postnatal day 7 (P7) were kept at high oxidation state (75 ± 5%) for 5 days before returned to normal environment. Retinal tissue was cut into sections. Oxygen induced retinal neovascularization and vascular structural changes were evaluated using retinal fluorescein angiography. The number of endothelial cell nuclei breaking through the retinal internal limiting membrane was counted after H&E staining. The mRNA expression levels of VEGF, αA- and αB-crystallins in the mouse retina were determined using real-time RT-PCR. The distribution of αA- and αB-crystallins in the retina was detected by fluorescent immunohistochemistry staining. Results: Oxygen induction triggered new blood vessel formation in the retina and impaired the structure of the retinal vascular network. The number of endothelial cell nuclei breaking through the retinal internal limiting membrane was significantly increased in the OIR group compared to the control group at P13, P17 and P21 ($P < 0.01$), reaching the peak on P17. The expression levels of VEGF, αA- and αB-crystalllins were also significantly different between the OIR and control groups. VEGF expression was highest on P15, αA-crystallin expression was highest on P17, whereas αB-crystallin expression kept increasing during the time frame of our study. Both αA- and αB-crystallins were expressed in the ganglion cell layer and the inner nuclear cell layer. While αA- and αB-crystallins were only located on the cell membrane in the outer ganglion cell layer, they were observed both on the cell membrane and in the cytoplasm in the inner layer of cells. Conclusion: Using our mouse model of oxygen-induced retinopathy, we showed that the expression patterns of VEGF, αA- and αB-crystallins during retinal neovascularization in both spatially and temporally manners, providing significant insights into the molecular mechanisms of retinopathy and the associated neovascularization.

Keywords: VEGF, αA-crystallin, αB-crystallin, oxygen induced retinopathy, gene expression pattern, mouse model, neovascularization

Introduction

Retinal neovascularization is an iconic change of diabetic retinopathy, age-related macular degeneration, retinopathy of premature infant, and other refractory ocular retinopathies. As one of the most important causes of blindness, extensive neovascularization results in decreased visual acuity and even retinal detachment. Therefore, it is essential to understand the molecular changes associated with the pathogenetic progress of retinal neovascularization and retinopathy, and provide important translational clues to improve therapeutic approaches.

Vascular endothelial growth factor (VEGF) is a potent promoter of angiogenesis involved in a wide variety of physiological and pathological processes [1]. Evidence from studies using anti-VEGF antisera [2], anti-VEGF aptamers [3], soluble VEGF receptor [4], human recombinant

VEGF [5], and VEGFR1-neutralizing antisera [6], has demonstrated the critical role of VEGF in retinal neovascularization. Currently, four anti-VEGF agents, including bevacizumab, ranibizumab, pegaptanib and aflibercept, are used via intravitreal injection for the treatment of neovascular retinal diseases.

A-crystallins belong to the small heat shock protein (sHSP) family. They contribute to the maintenance of cellular protein conformation in response to stress. Besides mediating protein folding, α-crystallins also play important roles in transmembrane transport, shift, and cytoskeletal stability. Recent microarray and proteomic studies have shown that crystallins were up-regulated during oxygen-induced retinopathy [7]. In addition, the expression of crystallins were found to be dysregulated in diabetic retinopathy, retinitis pigmentosa and other retinal disorders [8], further suggesting the pathogenic role of crystallins in retinopathy [9].

Although VEGF and crystallins have been identified in association with retinopathy, the temporal and spatial changes in their expression have not yet been determined. Herein, we studied the quantitative mRNA expression of VEGF, αA- and αB-crystallins, and the distribution of αA- and αB-crystallins in the retinal tissue from a mouse model of oxygen-induced retinopathy. Our results expand the current knowledge about the detailed molecular changes during the pathogenic process of retinopathy.

Materials and methods

Experimental animals

The 90 C57BL/6J rats, male and female, were raised in the animal room at the Public Health Academy of Tianjin Medical University, and were of the SPF grade. The neonatal rats were fed by female mice during lactation. All mice were then randomly divided into OIR group (experiencing a high oxygen concentration from P7 to P12) or control group (kept in normal atmospheric environment during the whole experiment), 45 mice in each group. For experiments involving animals, approval was obtained from the institutional review board of Tianjin Medical University. Informed consent was provided according to the Declaration of Helsinki.

Primers

The upstream primer for αA-crystallin was 5'-TCACCGTGAAGGTACTGGA-3', and the downstream primer was 5'-TCACCGTGAAGGTACTGGAGG-3'. The amplified fragment was 111 base pairs (bp). The upstream primer for αB-crystallin was 5'-TCCACGGCAAGCACGAAG-3' and the downstream primer was 5'-GACAGGGATGAAGTGATGGTGAG-3'. The amplified fragment was 115 bp. The upstream primer for VEGF was 5'-TAAATCCTGGAGCGTTCACTG-3', and the downstream primer was 5'-TCAAGCTGCCTCCGTTTAACT-3'. The amplified fragment was 115 bp. The upstream primer of β-actin was 5'-AGAGGGAAATCGTGCGTGAC-3', and the downstream primer was 5'-AGGCAGCTCATAGCTCTTCTCC-3'. The amplified fragment was 116 bp. The primer synthesis was authorized by the biotechnology limited company of TEDA College in Nan Kai University (Tianjin, China).

Establishment of the animal model of oxygen-induced retinopathy

C57BL/6J mice were fed with cage rearing starting from 3 days after birth (P3), and were randomly divided into OIR group and control group. According to Pierce et al [10], since P7 mice in the OIR group were moved into the feeding box where oxygen concentration was 75% ± 5% for 5 days. The temperature was 23 ± 2°C. The oxygen concentration was measured and controlled by the oxygen analyzer (BioSperix, New York, United States). On P12, the OIR group was returned to normal atmospheric environment. The mice in the control group were kept in normal atmospheric environment during the whole study, with all other conditions and schedules the same as the OIR group.

On P13, P17 and P21, three mice were randomly taken from each group to prepare retinal sections for H&E staining to examine retinal neovascularization. On P13, P15, P17, and P21, six mice were taken from each group to extract retinal tissue for analyzing the mRNA levels of VEGF, αA- and αB-crystallins and VEGF using real-time RT-PCR, in triplicate. Three mice from each group were taken randomly on P13, P15, P17 and P21 to prepare retinal sections for fluorescence immunohistochemistry (IHC) staining. The distribution of αA- and αB-crystallins in the retinal tissue of mice was also examined.

Retinal fluorescein (FITC) angiography

FITC angiography was performed as described with modification [11]. On P13, P17 and P21,

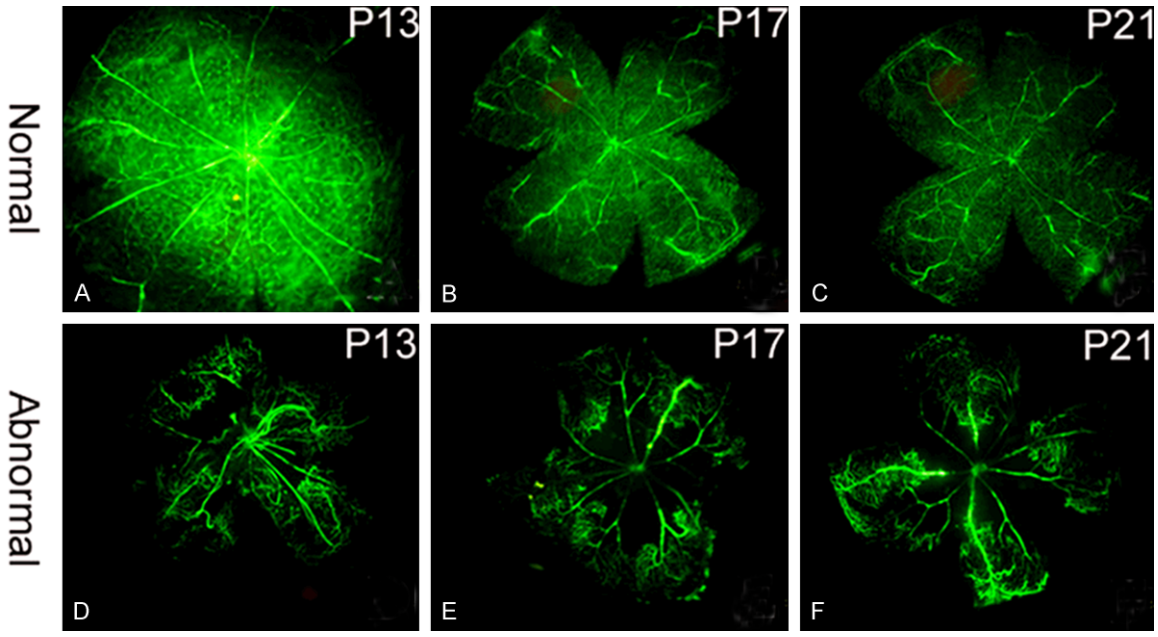

Figure 1. Retinal blood vessel formation shown by FITC angiography. A. Immature blood vessels in the control group on P13. B. Absence of immature blood vessels and peripheral capillaries in the control group on P17. C. Blood vessels were completely developed and reached the peripheral retinal areas in the control group on P21. D. Tortuous and disordered blood vessels with areas lacking fluorescence in the OIR group on P13. E. Expanded blood vessels and decreased branches, with newly formed capillaries and peripheral leakage in the OIR group on P17. F. Areas without fluorescence at the peripheral retina were still seen, but leakage was not observed in the OIR group on P21.

three mice from each group (OIR or control) were randomly selected for retinal FITC angiography. The mice were anesthetized using ether, and injected intracardially with 1 mL FITC isothiocyanate-labeled dextran (50 mg/mL, MW 2 × 10^6 Da). One hour later, the mice were euthanized, and their eyes were immediately extracted and fixed using 4% paraformaldehyde for 1-3 h. The eyes were cut from the edge of corneoscleral to separate the retinas. After mounted on glass slides, the retinas were examined and photographed under a fluorescence microscope.

H&E staining for analyzing retinal vascular proliferation

H&E staining was performed as described with modification [12]. Eyes were continuously sectioned from cornea to papillary, 6 μm each. A total of 10 pathological sections in each eye were used for staining. Ten high power fields (400×) in each section were used to count the number of vascular endothelial cells breaking through retinal internal limiting membrane, and to obtain the average numbers of the vascular endothelial cells breaking through the inner limiting membrane per slice. Only endothelial cells closely associated with the inner limiting membrane were counted, not including other vascular endothelial cells that did not reach the internal limiting membrane in the intravitreal.

Real-time RT-PCR

Real-time RT-PCR was performed as described with modification [13]. Eye balls in the OIR and the control groups were extracted under operation microscope. The cornea, lens, and vitreous body were removed and the retina tissue was taken out. Four retinal tissues were placed into 1 mL Trizol liquid. All samples were preserved in -80°C. Total RNA in retina was extracted using the one-step Trizol method. cDNA were synthesized using reverse transcription. The standard RT-PCR reaction system was constructed according to the operation manual. 1 μg cDNA was used as a template. The sample in each tube was repeated three times. After 2 min at 50°C and 10 min at 95°C, 40 cycles were performed (95°C for 15 s, 60°C for 1 min). Cycle threshold was then generated by automatic instrument (CT). Data were analyzed using $2^{-\Delta\Delta CT}$ method to calculate the αA-, αB-crystallins and VEGF mRNA abundance at each time point in both groups.

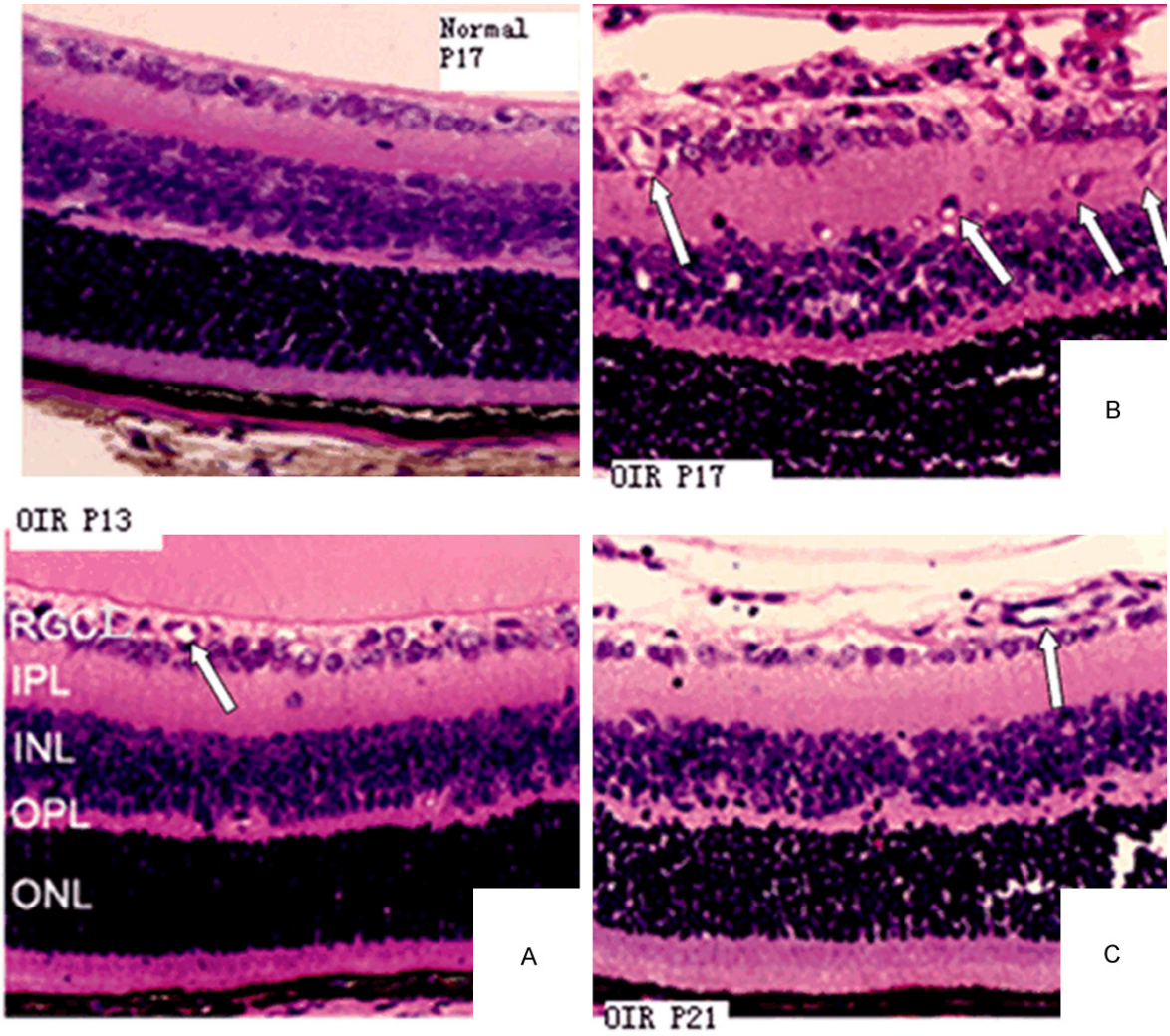

Figure 2. H&E staining of the retinas from the control group (P17) shows a limited number of vascular endothelial cells and the lumen-sample structure in retinal internal limiting membrane (400X). H&E staining of the retinas from the OIR group on P13, P17 and P21 (400×). A. On P13, the internal limiting membrane was integrated and blood vessels were dilated. B. On P17, the internal limiting membrane was not integrated. Large amounts of visible vascular endothelial cell nuclei, alone or clustered, broke through the retinal inner limiting membrane. C. On P21, the internal limiting membrane became smoother. The number of vascular endothelial cells breaking through the internal limiting membrane was significantly reduced. Arrows indicate newly formed blood vessels.

Fluorescence IHC staining of α-crystallins

Fluorescence IHC staining was performed as described with modification [14]. Six eye balls were removed from mice at P13, P15, P17 and P21, respectively, in the OIR and control groups. The lens tissue was removed from each eye. The eye balls were embedded in OCT, and sectioned from cornea to optic papilla, 6 μm each. The frozen sections were blocked using 5% bovine serum for 30 minutes, prior to the incubation with indicated antibodies (1:50) at 4°C overnight. Sections were then incubated with goat anti-mouse fluorescent IgG (H+L)-FITC (1:20) at 37°C for 1 hours, followed by sealing with 50% glycerol solution. The sections were examined using fluorescence microscopy.

Statistical analysis

SPSS13.0 software package was used for statistical analysis. All values were expressed as $\bar{x} \pm s$. When the variance was neat, data were analyzed using ANOVA and student t test. When the variance was not neat, we made approximate F test. The difference was considered sta-

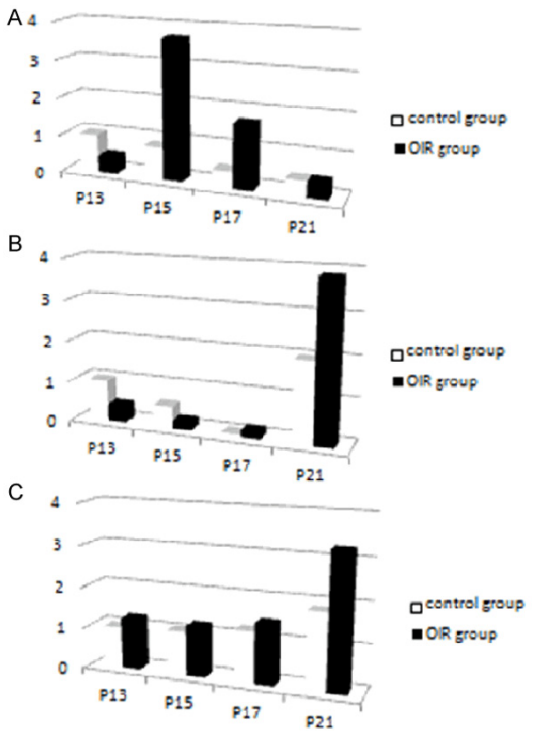

Figure 3. Dynamic comparison of the expression of (A) VEGF, (B) αA- and (C) αB-crystallins between the OIR and the control groups on P13, P15, P17, and P21. Calculated Ct values were shown.

tistically significant if $P < 0.05$. The difference was considered extremely statistically significant if $P < 0.01$.

Results

Oxygen induction impairs retinal vascular morphology and stimulates neovascularization

We compared the mouse retinal vascular morphology between the OIR and the control groups using FITC angiography. On P13 (the postnatal day 13), the retinas from the control group were not yet completely developed. Growing from the optic papilla, the blood vessels distributed evenly. Immature and developing capillaries were seen (**Figure 1A**). Compared with the control group, the retinal blood vessels in the OIR group on P13, one day after the OIR group left the anoxia environment, were tortuous and disordered, with a reduced number of branches (**Figure 1D**). Hyaloid arteries could still be seen. It is important to note that extensive areas with the absence of fluorescence at the center of the retinas were observed, indicating that there were occlusions. Capillaries were found at the peripheral areas of the retinas. In addition, neovascularization was only found in the outer layer of the retina, while no new capillary formation was seen in the inner layer. On P17 (the postnatal day 17), 5 days after the OIR group left the anoxia environment, the retinas in the control group showed mature blood vessels which replaced the previously observed immature vessels (**Figure 1B**). However, in the OIR group, the retinal blood vessels were significantly expanded, with a large amount of newly formed capillaries in a high density. The structure and distribution of these capillaries were significantly disordered. Compared to the control group, leakage at the peripheral retinal areas and a large number of vascular endothelial cells breaking through the retinal inner limiting membrane were observed. There were also extensive areas of occlusion (**Figure 1E**). On P21 (the postnatal day 21), 9 days after the OIR group left the anoxia environment, the retinal blood vessels in the control group reached the peripheral retinal areas, significantly different from those observed on P17 (**Figure 1C**). In the OIR group, retinal areas deficient of fluorescence that indicates occlusion were still seen, but the amount of newly formed capillaries was reduced. Leakage was not observed (**Figure 1F**).

Oxygen induction triggers vascular endothelial cells to break through the internal limiting membrane

On P13, P17 and P21 in control group, neovascular endothelial cell nuclei appeared occasionally. Only a small number of the vascular endothelial cells and the lumen-sample structure broke through the internal limiting membrane at P17 (**Figure 2**), indicating that during the development of retina, no abnormal proliferation of blood vessels happens under normal circumstance.

In OIR group on P13, vascular lacunas could be seen in both the retinal inner nuclear layer and the outer plexiform layer. Vascular expansion could be seen at the ganglion cell layer of retina (**Figure 3A**). On P17 in the OIR group, vascular lacunas increased in the retinal inner nuclear layer and the ganglion cell layer. The vascular lacunas and the new blood vessels were observed in the inner plexiform layer. The neovascularization and the vascular clusters gradually broke through internal limiting membrane in the retinal ganglion cell layer. Part of the neo-

Table 1. Numbers of vascular endothelial cell nuclei breaking through the inner limiting membrane at different time points in the OIR and the control groups

	OIR group (n = 3)	control group (n = 3)	*t*-value	*P*-value
P13	8.72 ± 2.53	0.63 ± 0.30	16.502	P < 0.01
P17	43.51 ± 12.15	1.33 ± 0.12	35.867	P < 0.01
P21	21.91 ± 3.27	0.56 ± 0.29	32.631	P < 0.01
F-value	33.561	0.985		
P	P < 0.01	P > 0.05		

vascularization breaking through the vitreous cavity grew along the posterior lens surface. The internal limiting membrane was not complete. Neovascularization reached the peak at the time point. Single or clusters of vascular endothelial cells were evident (**Figure 3B**). On P21, there were still traces of the vascular lacuna in the kernel layer of mouse retina disc, whereas the vascular lacuna in inner plexiform layer and the new blood vessels disappeared completely. Neovascularization and vascular clusters in the ganglion cell layer of retina breaking through internal limiting membrane have completely disappeared. The internal limiting membrane was not intact (**Figure 3C**). The numbers of vascular endothelial cells breaking through internal limiting membrane in OIR group on P13, P17 and P21, were significantly different than those in the control group (P < 0.01, **Table 1**).

Together, these results indicate that our model of retinal neovascularization was successfully established, and thus was used as the experimental model for studying the temporal and spatial expression of VEGF, αA- and αB-crystallins. P13, P15, P17, P21 were the time points when neovascularization began to form, reached the peak, and subsided, and were therefore used for other experiments.

The temporal change in the retinal expression levels of VEGF, αA- and αB-crystallns

Using real-time RT-PCR, we examined the dynamic changes in the mRNA levels of VEGF, αA- and αB-crystallins extracted from the retinal tissues of the OIR group and the control mice. The CT value was normalized referring to the β-actin gene. The data were calculated using the $2^{-\Delta\Delta CT}$ method.

After oxygen induction, the VEGF expression in OIR group increased and reached the peak at P15, followed by a gradual but significant reduction (F = 310.144, P < 0.01). The VEGF expression in the control group was highest on P13, and slowly decreased between P13 and P21, with a statistically significant difference among the studied time points (F = 66.365, P < 0.01). Compared to the control group, the VEGF expression in the OIR group on P13, P15 and P17 was significantly higher (t = 15.947, 54.223, 32.998, P < 0.01). The VEGF expression on P21 was slightly lower in the OIR group compared to that in the control group, but the difference was not statistically significant (t = 0.630, P > 0.05) (**Figure 4A**)

The αA-crystallin expression in the OIR group was decreased at the beginning after oxygen induction, but then substantially increased after P17, with a statistically significant difference (F = 632.299, P < 0.01). A similar temporal decrease-increase expression pattern was also observed in the control group (F = 204.149, P < 0.01). The αA-crystallin expression in the OIR group was significantly lower than that in the control group on P13 and P15, (t = 10.011, 13.342, P < 0.01), whereas on P17 and P21 its expression in the OIR group was significantly (t = 9.152, 9.205, P < 0.01) (**Figure 4B**).

The expression of αB-crystallin shows a gradually increasing trend in both the OIR (F = 410.393, P < 0.01) and the control groups (F = 11.106, P < 0.01). Its expression on P13, P15 and P17 in OIR group was significantly lower than that in control group (t = 8.693, 3.315, 3.176, 14.872, P < 0.01) (**Figure 4C**).

Oxygen induction disturbs the spatial distribution of α-crystallins in the retina

Besides the temporal dynamics of expression, we further studied the spatial distribution of α-crystallins with or without oxygen induction. The expression of αA- and αB-crystallins in the retinal tissue was observed in both the OIR and the control groups at all the time points we studies. The positively stained cells were mainly distributed in the retinal ganglion cell layer, the inner, and the outer nuclear layers. In the inner layer of cells, both αA- and αB- crystallins were expressed not only on the cell membrane but also expressed in the cytoplasm, whereas they were expressed only on the cell membrane

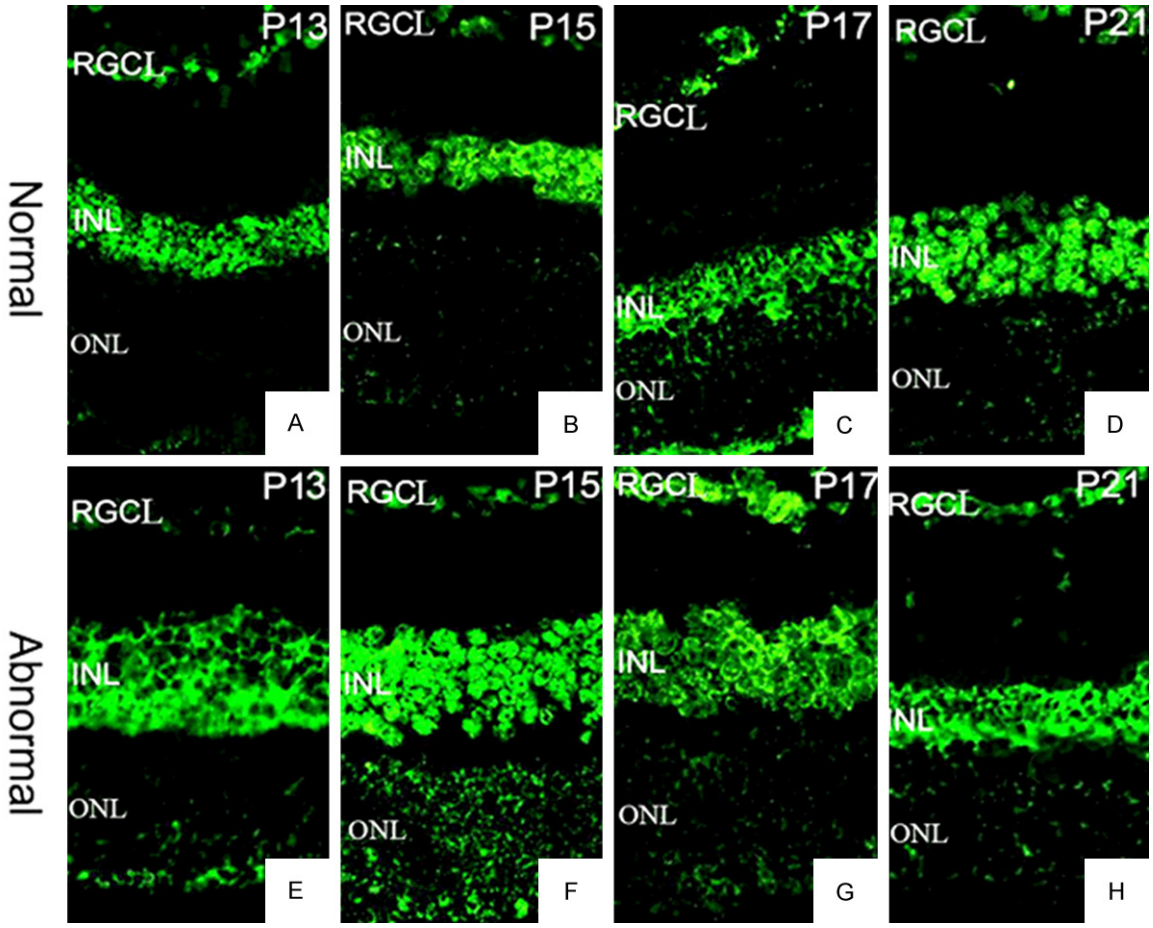

Figure 4. AA-crystallin expression and distribution in the retina on (A and E) P13, (B and F) P15, (C and G) P17, and (D and H) P21. Upper panel (A-D), control group. Lower panel (E-H), OIR group. 400×.

in the outer nuclear layer of cells (**Figures 4** and **5**). Both crystallins in the retinal tissue showed significant different patterns of distribution between the OIR and the control groups at each time point. In addition, these results showing the protein abundance of αA- and αB-crystallins were consistent with the mRNA expression data (**Figure 4**).

Discussion

The similar structure of retinal tissue between mouse and human makes mouse an important experimental animal model to study various human retinal diseases. In this study, we selected C57BL mice, whose retinal blood vessels share a high degree of similarities with those in human. We used a mouse model of oxygen induced retinopathy, a commonly used animal model of retinal neovascularization. Quantification of the retinal neovascularization is an important basis for studying retinopathies. Multiple methods have been developed to quantify retinal neovascularization induced by oxygen, such as counting the number of cell nuclei breaking through the inner limiting membrane in a serial of sections, counting the number of occluded vessels, loops and ridges of the capillary vessels, counting vascular density in the stretched retina (the method of 12:00 o'clock). Amount these methods, quantifying the vascular endothelial cell nuclei breaking through retinal inner limiting membrane in retinal tissue sections has been regarded as the gold standard for quantitative study of retinopathy [15]. In our study, we only counted those vascular endothelial cell nuclei closely associated with the retina to ensure that these numbers reflect the reliability of neovascularization in retina. In addition, H&E staining displays inner limiting membrane in retina and vascular endothelial cell nuclei breaking through inner limiting membrane, making the quantification relatively clear and accurate.

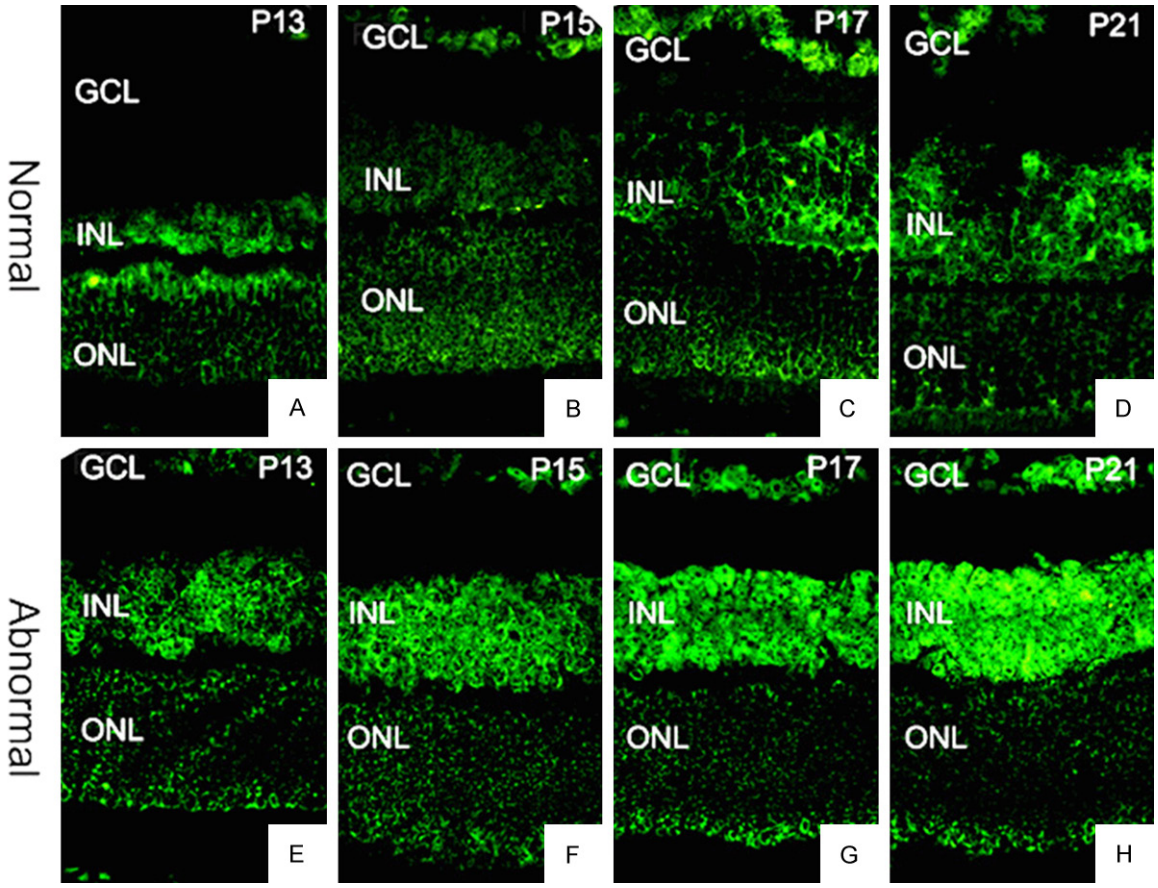

Figure 5. AB-crystallin expression and distribution in the retina on (A and E) P13, (B and F) P15, (C and G) P17, and (D and H) P21. Upper panel (A-D), control group. Lower panel (E-H), OIR group. 400×.

A-crystallins belongs to the small heat shock protein, and are highly expressed in cells with low mitotic activities, such as crystalline lens, myocardial and skeletal muscle. There are multiple different subtypes of crystallins expressed in the non lens tissues [16]. Although the subtypes of crystallins shared the same mechanisms of action, they show distinct distributions. Thermal and metabolic stress conditions threaten cell survival. Studies on enzymes that inhibit apoptosis suggests that αA- and αB-crystallins play a decisive protecting role in non lens tissues [17, 18], and the activities and expression of heat shock proteins could be used as a sensitive and reliable index of tissue ischemia. A-crystallins have a wide range of biological functions, among which acting as molecular chaperones is a critical function that prevents protein aggregation and degeneration, and supports cell survival [19]. A-crystallins has been reported to be up-regulated to protect retinal tissue from apoptosis in diabetic retinopathy [20]. AA-crystallin is particularly expressed in the retinal tissue of sympathetic ophthalmia, which further suggested its protective effects on the apoptosis triggered by the inflammatory cells [21].

In this study, we reported the difference among the retinal expression patterns of VEGF, αA- and αB-crystallins. The expression level of VEGF in the OIR retina after oxygen induction was significantly higher than that in control group. Such an increase in VEGF expression was transient, because VEGF was down-regulated when the new blood vessels formed to alleviate hypoxia. However, αA-crystallin showed an opposite expression trend compared to VEGF, while the expression of αB-crystallin significantly increased during the neovascular process. Therefore, αA- and αB-crystallin may be associated with the formation of new blood vessels in our mouse model of oxygen induced retinopathy. In addition, αA- and αB-crystallins could protect retinal tissue from hypoxia-induced injury that leads to apoptosis [22]. The

role of α-crystallins in regulating angiogenesis has been recently intensively studied. AB-crystallin and HSP27 have been shown to support angiogenesis by promoting vascular survival during tube morphogenesis [23]. Silencing αB-crystallin in the oxygen-induced retinopathy resulted in significant decrease in the formation of new blood vessels [24]. Another study reported that suture or chemical burns induced corneal neovascularization in mice was attenuated by subconjunctival injection of αA-crystallin. It was suggested that αA-crystallin mediates the expression of VEGFR-1 [25]. Additionally, during the early stage of autoimmune disease uveitis, αA-crystallin was up-regulated in the inner segments of the photoreceptor, and inhibited mitochondrial oxidative stress-induced apoptosis, further suggesting its anti-inflammatory role [26]. Moreover, there is a strong relationship between inflammation and angiogenesis [27, 28], and α-crystallins may serve as a bridge connecting these two biological events. Further studies are needed to determine their detailed molecular mechanics.

Out results showed that the expression of αA- and αB-crystallins were both found in the retinal tissue of the OIR and the control group, and mainly located in the ganglion cell layer, inner and outer nuclear layers of cells. The kernel layer cells not only expressed αA- and αB-crystallins on the cell membrane but also in the cytoplasm, whereas the outer nuclear layer of cells only expressed αA- and αB-crystallins on the cell membrane. These results are consistent with a previous study published in 2003 by Xi et al [29], which showed that there were 20 different crystallins expressed in retina of mouse under physiological conditions, and αA-crystallin was expressed in both the outer and inner nuclear layers. The results of this study also agree with another study reporting that the αA- crystallin expression was increased in the retina tissue in the early experimental allergic uveitis [26]. Our study not only confirmed the expression of α-crystallins in the mouse retina, but also examined the temporal and spatial expression of the αA- and αB-crystallins in a mouse model of oxygen induced retinopathy. Our results provide important insights into the relationship between α-crystallins and neovascularization in oxygen-induced retinopathy.

It is known that αB-crystallin is expressed in the neovessels of epiretinal membrane in human proliferative diabetic retinopathy (Retina 2012; 32: 1190-6). The immunolocalization of α-crystallins in the microvessels among P13~P21 in both groups was evaluated, and the results were consistent with previous investigation.

Currently there are only limited treatments for retinal neovascularization, including mainly laser photocoagulation, vitrectomy surgery cutting extra fiber vascular membrane, and anti-angiogenesis medicines. To improve the clinical outcome, it is necessary to develop new medicines that suppress the pathological retinal neovascularization. Our study suggest that αA- and αB-crystallins may be involved in the occurrence and development of retinal angiogenesis. They may have a protective effect on the mouse retinal tissue where oxygen induced retinopathy, which needs further mechanistic studies.

Acknowledgements

This study was supported by Tianjin Education Scientific Research Projects (20140136).

Disclosure of conflict of interest

None.

Address correspondence to: Xiao-Rong Li, Tianjin Medical University Eye Hospital, School of Optometry and Ophthalmology, Tianjin Medical University Eye Institute, Tianjin Medical University, NO. 251 Fukang Road, Nankai District, Tianjin 300384, China. Tel: 86-022-58280808; Fax: 86-022-58286434; E-mail: xiaorongli201410@126.com

References

[1] Ferrara N. Vascular endothelial growth factor: basic science and clinical progress. Endocr Rev 2004; 25: 581-611.

[2] Adamis AP, Shima DT, Tolentino MJ, Gragoudas ES, Ferrara N, Folkman J, D'Amore PA and Miller JW. Inhibition of vascular endothelial growth factor prevents retinal ischemia-associated iris neovascularization in a nonhuman primate. Arch Ophthalmol 1996; 114: 66-71.

[3] Robinson GS, Pierce EA, Rook SL, Foley E, Webb R and Smith LE. Oligodeoxynucleotides inhibit retinal neovascularization in a murine model of proliferative retinopathy. Proc Natl Acad Sci U S A 1996; 93: 4851-4856.

[4] Aiello LP, Pierce EA, Foley ED, Takagi H, Chen H, Riddle L, Ferrara N, King GL and Smith LE. Suppression of retinal neovascularization in

vivo by inhibition of vascular endothelial growth factor (VEGF) using soluble VEGF-receptor chimeric proteins. Proc Natl Acad Sci U S A 1995; 92: 10457-10461.
[5] Tolentino MJ, Miller JW, Gragoudas ES, Chatzistefanou K, Ferrara N and Adamis AP. Vascular endothelial growth factor is sufficient to produce iris neovascularization and neovascular glaucoma in a nonhuman primate. Arch Ophthalmol 1996; 114: 964-970.
[6] Ozaki H, Seo MS, Ozaki K, Yamada H, Yamada E, Okamoto N, Hofmann F, Wood JM and Campochiaro PA. Blockade of vascular endothelial cell growth factor receptor signaling is sufficient to completely prevent retinal neovascularization. Am J Pathol 2000; 156: 697-707.
[7] Kim SJ, Jin J, Kim YJ, Kim Y and Yu HG. Retinal proteome analysis in a mouse model of oxygen-induced retinopathy. J Proteome Res 2012; 11: 5186-5203.
[8] Arrigo AP and Simon S. Expression and functions of heat shock proteins in the normal and pathological mammalian eye. Curr Mol Med 2010; 10: 776-793.
[9] Yaung J, Kannan R, Wawrousek EF, Spee C, Sreekumar PG and Hinton DR. Exacerbation of retinal degeneration in the absence of alpha crystallins in an in vivo model of chemically induced hypoxia. Exp Eye Res 2008; 86: 355-365.
[10] Pierce EA, Avery RL, Foley ED, Aiello LP and Smith LE. Vascular endothelial growth factor/vascular permeability factor expression in a mouse model of retinal neovascularization. Proc Natl Acad Sci U S A 1995; 92: 905-909.
[11] Ramirez M, Wu Z, Moreno-Carranza B, Jeziorski MC, Arnold E, Diaz-Lezama N, Martinez de la Escalera G, Colosi P and Clapp C. Vasoinhibin gene transfer by adenoassociated virus type 2 protects against VEGF- and diabetes-induced retinal vasopermeability. Invest Ophthalmol Vis Sci 2011; 52: 8944-8950.
[12] Yamada R, Kostova MB, Anchoori RK, Xu S, Neamati N and Khan SR. Biological evaluation of paclitaxel-peptide conjugates as a model for MMP2-targeted drug delivery. Cancer Biol Ther 2010; 9: 192-203.
[13] Xu S, Oshima T, Imada T, Masuda M, Debnath B, Grande F, Garofalo A and Neamati N. Stabilization of MDA-7/IL-24 for colon cancer therapy. Cancer Lett 2013; 335: 421-430.
[14] Xu S, Grande F, Garofalo A and Neamati N. Discovery of a novel orally active small-molecule gp130 inhibitor for the treatment of ovarian cancer. Mol Cancer Ther 2013; 12: 937-949.
[15] Chikaraishi Y, Shimazawa M and Hara H. New quantitative analysis, using high-resolution images, of oxygen-induced retinal neovascularization in mice. Exp Eye Res 2007; 84: 529-536.
[16] McGreal RS, Kantorow WL, Chauss DC, Wei J, Brennan LA and Kantorow M. alphaB-crystallin/sHSP protects cytochrome c and mitochondrial function against oxidative stress in lens and retinal cells. Biochim Biophys Acta 2012; 1820: 921-930.
[17] Wolf L, Yang Y, Wawrousek E and Cvekl A. Transcriptional regulation of mouse alpha A-crystallin gene in a 148kb Cryaa BAC and its derivates. BMC Dev Biol 2008; 8: 88.
[18] Rao NA, Saraswathy S, Pararajasegaram G and Bhat SP. Small heat shock protein alphaA-crystallin prevents photoreceptor degeneration in experimental autoimmune uveitis. PLoS One 2012; 7: e33582.
[19] Ahmad MF, Raman B, Ramakrishna T and Rao Ch M. Effect of phosphorylation on alpha B-crystallin: differences in stability, subunit exchange and chaperone activity of homo and mixed oligomers of alpha B-crystallin and its phosphorylation-mimicking mutant. J Mol Biol 2008; 375: 1040-1051.
[20] Kase S, Ishida S and Rao NA. Increased expression of alphaA-crystallin in human diabetic eye. Int J Mol Med 2011; 28: 505-511.
[21] Kase S, Meghpara BB, Ishida S and Rao NA. Expression of alpha-crystallin in the retina of human sympathetic ophthalmia. Mol Med Rep 2012; 5: 395-399.
[22] Christopher KL, Pedler MG, Shieh B, Ammar DA, Petrash JM and Mueller NH. Alpha-crystallin-mediated protection of lens cells against heat and oxidative stress-induced cell death. Biochim Biophys Acta 2014; 1843: 309-315.
[23] Dimberg A, Rylova S, Dieterich LC, Olsson AK, Schiller P, Wikner C, Bohman S, Botling J, Lukinius A, Wawrousek EF and Claesson-Welsh L. alphaB-crystallin promotes tumor angiogenesis by increasing vascular survival during tube morphogenesis. Blood 2008; 111: 2015-2023.
[24] Kase S, He S, Sonoda S, Kitamura M, Spee C, Wawrousek E, Ryan SJ, Kannan R and Hinton DR. alphaB-crystallin regulation of angiogenesis by modulation of VEGF. Blood 2010; 115: 3398-3406.
[25] Zhu W, Qi X, Ren S, Jia C, Song Z and Wang Y. alphaA-crystallin in the pathogenesis and intervention of experimental murine corneal neovascularization. Exp Eye Res 2012; 98: 44-51.
[26] Rao NA, Saraswathy S, Wu GS, Katselis GS, Wawrousek EF and Bhat S. Elevated retina-specific expression of the small heat shock protein, alphaA-crystallin, is associated with photoreceptor protection in experimental uve-

itis. Invest Ophthalmol Vis Sci 2008; 49: 1161-1171.
[27] Arroyo AG and Iruela-Arispe ML. Extracellular matrix, inflammation, and the angiogenic response. Cardiovasc Res 2010; 86: 226-235.
[28] Costa C, Incio J and Soares R. Angiogenesis and chronic inflammation: cause or consequence? Angiogenesis 2007; 10: 149-166.
[29] Xi J, Farjo R, Yoshida S, Kern TS, Swaroop A and Andley UP. A comprehensive analysis of the expression of crystallins in mouse retina. Mol Vis 2003; 9: 410-419.